Supplementary Information for:

Clinical Microfluidics for Neutrophil Genomics and Proteomics

Kenneth T. Kotz, Wenzong Xiao, Carol Miller-Graziano, Wei-Jun Qian, Aman Russom, Elizabeth A. Warner, Lyle L. Moldawer, Asit De, Paul E. Bankey, Brianne O. Petritis, David G. Camp II, Alan E. Rosenbach, Jeremy Goverman, Shawn P. Fagan, Bernard H. Brownstein, Daniel Irimia, Weihong Xu, Julie Wilhelmy, Michael N. Mindrinos, Richard D. Smith, Ronald W. Davis, Ronald G. Tompkins, Mehmet Toner, and the Inflammation and the Host Response to Injury Collaborative Research Program.

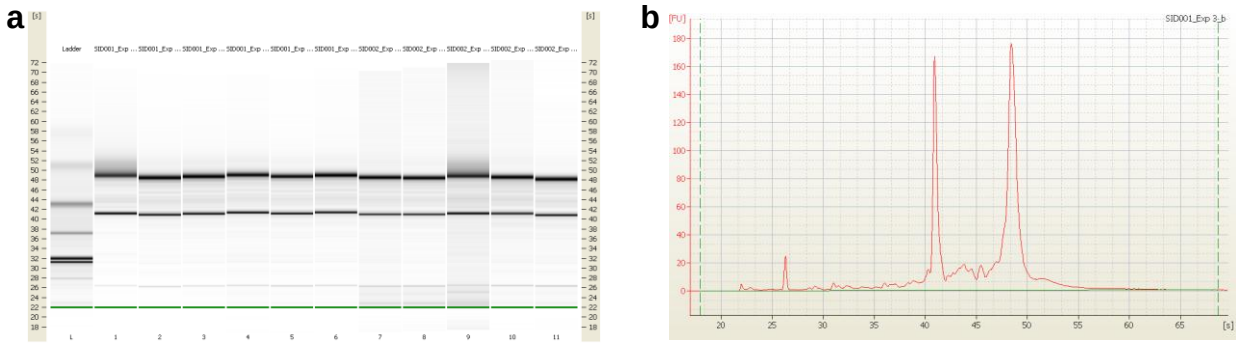

Supplementary Figure 1. Representative RNA electropherograms derived from microfluidic isolated PMNs recorded on an Agilent Bioanalyzer 2000. (**a**) RNA traces from two different burn patients at two different time points. Samples were run in triplicate (except for last sample run in duplicate). (**b**) Sample electropherogram from (**a**) with RIN = 9.5.

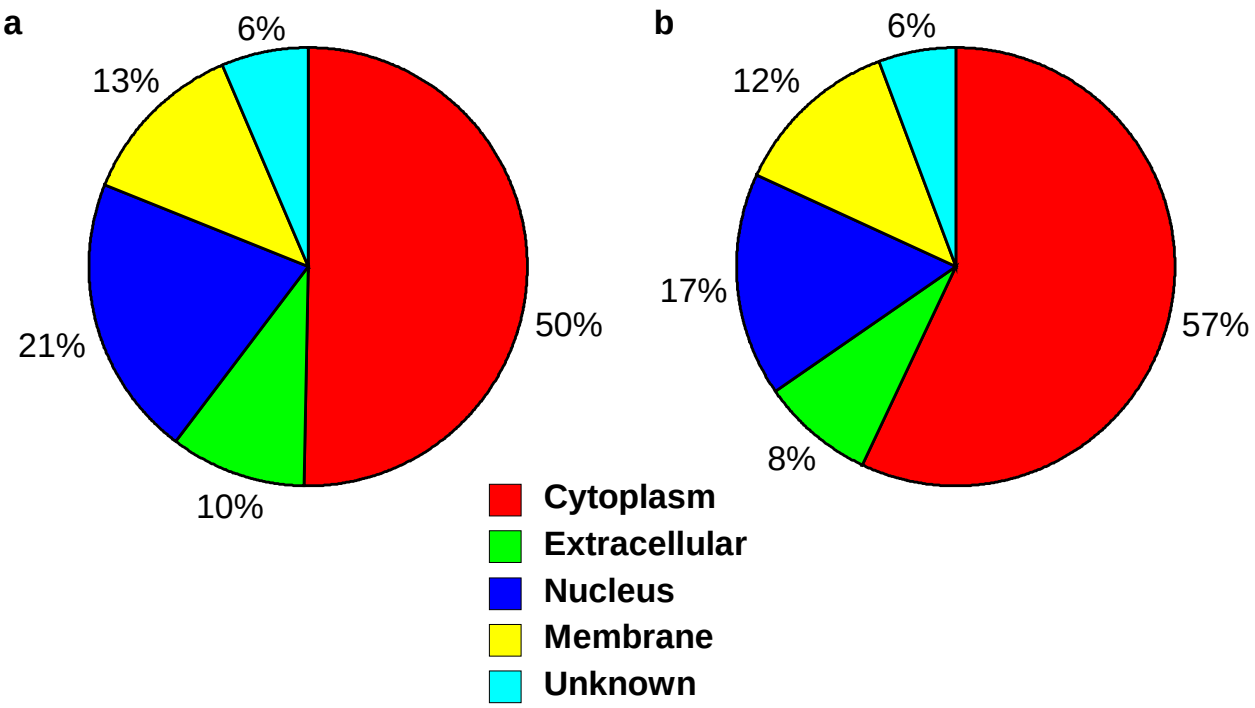

Supplementary Figure 2. Distribution of proteins identified by LC-MS based proteomics from granulocytes pre-processed with (**a**) microfluidics or (**b**) bulk isolation.

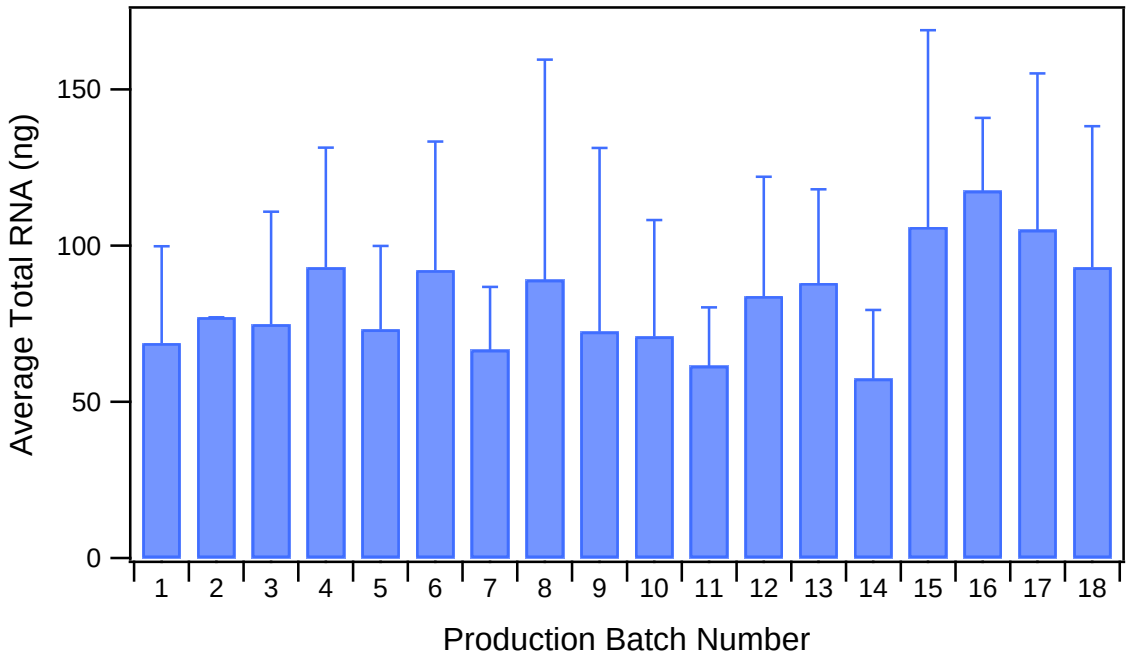

Supplementary Figure 3. Average total RNA isolated from microfluidic processed PMNs at all the clinical sites for each cassette production batch. Bar height represents is the mean total RNA with error bar representing one standard deviation. The differences between batches are not statistically significant at $P<0.05$ when analyzed with a 2-way ANOVA (fixed effect model) test.

Supplementary Table 1. Summary of on-chip characterization

Sample	Number of Cassettes Analyzed	Total number cells counted	Method†	% Gran	% Neutro	% MO	% Lymph
Ex vivo Stimulation Experiment							
Unstimulated	2	4160	IF	98	ND	ND	ND
LPS	2	1292	IF	98	ND	ND	ND
G+I	2	1020	IF	97	ND	ND	ND
Unstimulated	2	986	WG	98.6	95.9	1.2	0.3
LPS	2	346	WG	96.0	95.1	0.3	3.8
G+I	2	292	WG	96.2	96.2	0.3	3.1
MGH BURN	5	2058	WG/IF	96.6	96.2	0.5	3
Normals	6	1402	WG/IF	96.9	95.7	2	0.8

† On-chip cell purity was assessed by immunofluorescence (IF) or Wright-Giemsa (WG) staining. For IF, cells were considered granulocytes if they were CD66+ and DAPI+. Granulocytes were differentiated between eosinophils and neutrophils using WG.

Supplementary Table 2. Summary of proteomic lysis conditions

Lysis Method	Peptides	Proteins
UREA (6M)	700	364
Hypotonic (25 mM NH_4HCO_3)	610	207
50% TFE in 25 mM NH_4HCO_3	1985	560

Supplementary Table 4. Functional pathways following *ex vivo* stimulation.

	LPS vs. CTRL	GM+I vs. CTRL	LPS vs. GM+I
Canonical Pathways	**-Log(P-value) (Genes)**	**-Log(P-value) (Genes)**	**-Log(P-value) (Genes)**
TREM1 Signaling	10.5	10.2	3.09
Glucocorticoid Receptor Signaling	10.1		3.15
IL-10 Signaling	9.7	6.02	1.59
Death Receptor Signaling	8.58	5.06	
Role of Pattern Recognition Receptors in Recognition of Bacteria and Viruses	8.24	7.02	3.25
IL-6 Signaling	7.74	4.03	
PPARÎ±/RXRÎ± Activation	7.45	3.41	
IL-8 Signaling	7.37	6.25	2.47
Chemokine Signaling	7.22	9.33	
B Cell Receptor Signaling	6.89	7.29	
Hepatic Fibrosis / Hepatic Stellate Cell Activation	6.81	2.69	1.73
Acute Phase Response Signaling	6.75	4.89	
Activation of IRF by Cytosolic Pattern Recognition Receptors	6.66	5.58	
PPAR Signaling	6.52	3.13	
Role of NFAT in Regulation of the Immune Response	5.86	6.11	3.12
4-1BB Signaling in T Lymphocytes	5.62	4.61	
IL-17 Signaling	5.43	4.19	1.78
Aryl Hydrocarbon Receptor Signaling	5.42	4.75	2.02
Hypoxia Signaling in the Cardiovascular System	5.29	5.88	1.53
Toll-like Receptor Signaling	4.93	4.55	
Erythropoietin Signaling	4.92	5.16	
Role of PKR in Interferon Induction and Antiviral Response	4.7	5.03	
VEGF Signaling	4.63	5.15	
CD27 Signaling in Lymphocytes	4.4	4.59	
Apoptosis Signaling	4.25	3.78	
fMLP Signaling in Neutrophils	4.21	3.97	1.83
B Cell Activating Factor Signaling	4.2	3.31	
NF-ÎºB Signaling	4.12	3.62	
IL-3 Signaling	4.06	3.92	
Oncostatin M Signaling	4.01	3.14	
PDGF Signaling	3.96	3.27	
PI3K/AKT Signaling	3.92	7.25	
IL-2 Signaling	3.82	3.4	
CD40 Signaling	3.77	4.74	
Interferon Signaling	3.77	3.73	
p38 MAPK Signaling	3.74	2.66	
IL-12 Signaling and Production in Macrophages	3.64	3.09	2.23
Hepatic Cholestasis	3.58		
Integrin Signaling	3.51	2.19	
Ceramide Signaling	3.5	6.87	
Induction of Apoptosis by HIV1	3.48	4.9	
RAR Activation	3.43	4.35	
CCR3 Signaling in Eosinophils	3.43	1.44	
CXCR4 Signaling	3.4	3.43	
JAK/Stat Signaling	3.38	3.74	
14-3-3-mediated Signaling	3.32	3.12	
LPS-stimulated MAPK Signaling	3.31	3.93	
Role of RIG1-like Receptors in Antiviral Innate Immunity	3.22	2.92	
G-Protein Coupled Receptor Signaling	3.17	2.86	
Protein Ubiquitination Pathway	3.06	6.93	1.79
NRF2-mediated Oxidative Stress Response	3.02	6.65	2
Synaptic Long Term Potentiation	3.02		
IL-15 Signaling	3	2.96	
EGF Signaling	3	2.23	
CCR5 Signaling in Macrophages	3	1.45	

VDR/RXR Activation	2.98	2.79	
Î±-Adrenergic Signaling	2.97		
T Cell Receptor Signaling	2.94	2.89	
GM-CSF Signaling	2.92	4.83	
BMP signaling pathway	2.73	1.59	
Ephrin Receptor Signaling	2.68		
IGF-1 Signaling	2.66	3.57	
Neuregulin Signaling	2.66	2.33	
Xenobiotic Metabolism Signaling	2.55	3.03	
Huntington's Disease Signaling	2.55	2.7	2.81
CD28 Signaling in T Helper Cells	2.5	4.3	1.91
MIF Regulation of Innate Immunity	2.5	2.27	
NF-ÎºB Activation by Viruses	2.48	2.68	
IL-22 Signaling	2.45	2.52	
TGF-Î² Signaling	2.45	1.35	
LXR/RXR Activation	2.44	1.38	
IL-4 Signaling	2.41	3.7	2.69
Caveolar-mediated Endocytosis	2.23		
Pentose Phosphate Pathway	2.2		1.48
Lymphotoxin Î² Receptor Signaling	2.19	3.1	
Sphingolipid Metabolism	2.15	4.37	2.78
Eicosanoid Signaling	2.15		
PTEN Signaling	2.13	1.85	
cAMP-mediated Signaling	2.12		
Insulin Receptor Signaling	2.03	2.44	
Inositol Phosphate Metabolism	1.99	2.27	
Chondroitin Sulfate Biosynthesis	1.94		
Airway Pathology in Chronic Obstructive Pulmonary Disease	1.92		
p53 Signaling	1.91	3.03	
IL-9 Signaling	1.9	2.32	1.57
ERK/MAPK Signaling	1.85	1.77	
Leukocyte Extravasation Signaling	1.85		
Thrombopoietin Signaling	1.8	1.85	
T Helper Cell Differentiation	1.72	3.24	2.91
FcÎ³ Receptor-mediated Phagocytosis in Macrophages and Monocytes	1.71	1.76	1.69
Antigen Presentation Pathway	1.69	7.27	7.46
Estrogen Receptor Signaling	1.69	2.18	
N-Glycan Degradation	1.69		
Nitric Oxide Signaling in the Cardiovascular System	1.65		
Glycerophospholipid Metabolism	1.6		
Neurotrophin/TRK Signaling	1.55	1.84	
Natural Killer Cell Signaling	1.54	1.51	
Calcium Signaling	1.53		
Calcium-induced T Lymphocyte Apoptosis	1.45	2.01	2.07
Notch Signaling	1.41	1.73	1.32
FcÎ³RIIB Signaling in B Lymphocytes	1.41		
Role of BRCA1 in DNA Damage Response	1.39	2.72	
N-Glycan Biosynthesis	1.39	1.53	
Keratan Sulfate Biosynthesis	1.39		
SAPK/JNK Signaling	1.38	1.45	
Aminophosphonate Metabolism	1.36	2.22	
FGF Signaling	1.32	1.45	
Cytotoxic T Lymphocyte-mediated Apoptosis of Target Cells		2.33	
Glycerolipid Metabolism		2.32	
Glycosphingolipid Biosynthesis - Globoseries		2.09	
Pyrimidine Metabolism		2.01	
Cell Cycle: G1/S Checkpoint Regulation		1.95	1.83
Arginine and Proline Metabolism		1.83	2.95
CTLA4 Signaling in Cytotoxic T Lymphocytes		1.7	
Glycosphingolipid Biosynthesis - Ganglioseries		1.53	
Aminoacyl-tRNA Biosynthesis		1.5	
Endoplasmic Reticulum Stress Pathway		1.45	
Lysine Biosynthesis		1.43	5.1
One Carbon Pool by Folate		1.43	
Fc Epsilon RI Signaling		1.32	
Ubiquinone Biosynthesis			4.73
Mitochondrial Dysfunction			3.81
Nitrogen Metabolism			3.07
Oxidative Phosphorylation			2.57
Citrate Cycle			2.4

D-glutamine and D-glutamate Metabolism	1.89
Purine Metabolism	1.83
Nicotinate and Nicotinamide Metabolism	1.77
Glutathione Metabolism	1.39
Glutamate Metabolism	1.32

Supplementary Table 7. Summary of clinical cassette deployment

Sites (Sample Types)[a]	Seattle Harborview (T&B) University of Texas Medical Branch (B) University of Texas Southwestern (B&T) Loyola Medical Center (T) University of Pittsburg (T) University of Florida (B&T)
Total Isolations	1215
Total Extractions	867
Total RNA (ng)	81 ± 42
RNA Quality (RIN)	8.4± 0.6

[a] T denotes trauma patients, B denotes burn patients

Supplementary Table 9. Functional pathways derived from the gene expression data from trauma subjects.

Ingenuity Canonical Pathways from Upregulated Genes	-Log(P-value)	Ingenuity Canonical Pathways from Downregulated Genes	-Log(P-value)
Oxidative Phosphorylation	16.20	Antigen Presentation Pathway	4.02
Mitochondrial Dysfunction	10.3	IL-4 Signaling	3.3
Ubiquinone Biosynthesis	6.96	GNRH Signaling	2.92
Polyamine Regulation in Colon Cancer	6.34	Retinoic acid Mediated Apoptosis Signaling	2.81
Protein Ubiquitination Pathway	5.78	Interferon Signaling	2.65
Inositol Metabolism	4.88	Corticotropin Releasing Hormone Signaling	2.64
Pyrimidine Metabolism	3.85	Death Receptor Signaling	2.55
RAN Signaling	3.7	B Cell Receptor Signaling	2.45
Mitotic Roles of Polo-Like Kinase	3.58	Huntington's Disease Signaling	2.44
N-Glycan Biosynthesis	3.18	IL-3 Signaling	2.37
mTOR Signaling	3.14	ATM Signaling	2.33
EIF2 Signaling	2.99	Type I Diabetes Mellitus Signaling	2.24
Purine Metabolism	2.76	Molecular Mechanisms of Cancer	2.19
Pentose Phosphate Pathway	2.61	iCOS-iCOSL Signaling in T Helper Cells	2.16
Toll-like Receptor Signaling	2.55	FLT3 Signaling in Hematopoietic Progenitor Cells	2.15
Cell Cycle Regulation by BTG Family Proteins	2.52	Circadian Rhythm Signaling	2.01
Methane Metabolism	2.45	p38 MAPK Signaling	1.96
Nicotinate and Nicotinamide Metabolism	2.39	IL-15 Production	1.95
Role of BRCA1 in DNA Damage Response	2.33	p53 Signaling	1.94
NRF2-mediated Oxidative Stress Response	2.28	Cellular Effects of Sildenafil (Viagra)	1.9
Hypoxia Signaling in the Cardiovascular System	2.27	NF-κB Activation by Viruses	1.89
Glycolysis/Gluconeogenesis	2.24	Inositol Phosphate Metabolism	1.81
Mechanisms of Viral Exit from Host Cells	2.02	Production of Nitric Oxide and Reactive Oxygen Species in Macrophages	1.79
Cell Cycle: G2/M DNA Damage Checkpoint Regulation	1.91	Calcium-induced T Lymphocyte Apoptosis	1.79
Propanoate Metabolism	1.85	DNA Methylation and Transcriptional Repression Signaling	1.73
Pyruvate Metabolism	1.85	Role of NFAT in Regulation of the Immune Response	1.73
IGF-1 Signaling	1.81	CREB Signaling in Neurons	1.73
p70S6K Signaling	1.79	Lymphotoxin β Receptor Signaling	1.71
Butanoate Metabolism	1.77	Sphingolipid Metabolism	1.69
Aminoacyl-tRNA Biosynthesis	1.77	Protein Ubiquitination Pathway	1.67
Synthesis and Degradation of Ketone Bodies	1.76	CD28 Signaling in T Helper Cells	1.65
Inositol Phosphate Metabolism	1.71	HGF Signaling	1.65
Renal Cell Carcinoma Signaling	1.7	LPS-stimulated MAPK Signaling	1.63
Fcγ Receptor-mediated Phagocytosis in Macrophages and Monocytes	1.69	Nitric Oxide Signaling in the Cardiovascular System	1.58
Caveolar-mediated Endocytosis Signaling	1.63	IL-9 Signaling	1.55
Amyloid Processing	1.61	Calcium Signaling	1.52
Clathrin-mediated Endocytosis Signaling	1.6	Pancreatic Adenocarcinoma Signaling	1.51
Pancreatic Adenocarcinoma Signaling	1.55	Relaxin Signaling	1.5
PI3K/AKT Signaling	1.55	Aldosterone Signaling in Epithelial Cells	1.5
Stilbene, Coumarine and Lignin Biosynthesis	1.42	Synaptic Long Term Potentiation	1.49
Folate Biosynthesis	1.41	Thrombin Signaling	1.48
Role of CHK Proteins in Cell Cycle Checkpoint Control	1.36	Activation of IRF by Cytosolic Pattern Recognition Receptors	1.48
		CXCR4 Signaling	1.47
		April Mediated Signaling	1.47
		Glucocorticoid Receptor Signaling	1.45
		FGF Signaling	1.45
		Induction of Apoptosis by HIV1	1.4
		Lysine Biosynthesis	1.35
		B Cell Activating Factor Signaling	1.32
		Purine Metabolism	1.31

Supplementary Table 10. Comparison of gene expression and protein abundance for genes and proteins known to interact with LPS.

Gene Symbol	Gene Log2Ratio (LPS/Ctrl)	Protein Log2Ratio (LPS/Ctrl)	Gene Q-value(%)	Protein Q-value(%)	Annotation
ANXA5	2.92	0.67	0.00	2.79	Annexin A5
CYBA	1.38	0.57	0.58	1.16	cytochrome b-245, alpha polypeptide
CYBB	1.83	0.94	0.06	1.31	cytochrome b-245, beta polypeptide
EHD1	1.57	0.46	0.58	3.50	EH-domain containing 1
ENO1	1.60	0.11	0.37	1.95	enolase 1, alpha
FLOT2	-2.50	-2.91	0.00	0.95	flotillin 2
HSP90B1	2.42	0.87	0.00	2.34	heat shock protein 90kDa beta (Grp94), member 1
HSPA5	1.76	0.47	0.00	4.72	heat shock 70kDa protein 5 (glucose-regulated protein, 78kDa)
LCN2	2.75	-1.72	0.03	1.07	lipocalin 2
MMP9	-2.01	-2.57	0.10	0.09	Matrix metallopepsidase 9 (gelatinase B, 92kDa gelatinase, 92kDa type IV collagenase)
PBEF1	1.15	1.11	0.37	1.53	Nicotonamide phosphoribosyltransferase
RANBP2	2.42	-4.67	0.03	0.52	RAN binding protein 2
S100A9	-1.43	-0.72	0.00	3.96	S100 calcium binding protein A9
TALDO1	-1.61	0.41	0.13	3.52	transaldolase 1
VAV1	1.41	1.54	0.00	0.22	vav 1 guanine nucleotide exchange factor

Supplementary Table 11. List of all significant genes and proteins that show opposite directional changes following LPS stimulation.

Gene	Gene Log2Ratio (LPS/Ctrl)	Protein Log2Ratio (LPS/Ctrl)	Annotation
NCL	1.241	-4.852	Nucleolin
RANBP2	2.124	-4.667	RAN binding protein 2
PDIA6	1.193	-3.255	protein disulfide isomerase family A, member 6
MAP2K1IP1	1.210	-2.374	mitogen-activated protein kinase kinase 1 interacting protein 1
USO1	1.458	-1.799	USO1 homolog, vesicle docking protein (yeast)
LCN2	2.515	-1.723	lipocalin 2
SH3BGRL3	-1.357	1.000	SH3 domain binding glutamic acid-rich protein like 3
SLC9A3R1	-2.653	1.635	solute carrier family 9 (sodium/hydrogen exchanger), member 3 regulator 1
ARHGEF6	-2.419	2.235	Rac/Cdc42 guanine nucleotide exchange factor (GEF) 6
HIST1H2BK	-2.237	3.019	histone cluster 1, H2bk

Supplementary Table 12. Demographics for all trauma subjects included in microarray analysis of Figure 4. Data is presented as means ± SD or percentages.

Number patients/controls	26 / 10
Gender (M/F)	67% / 33%
Age (years)	38 ± 13
Maximal ISS Score	34 ± 10
Apache II Score	29 ± 7
Hospital length of stay (days)	38 ± 44

Supplementary Methods

Study Subjects and Blood Sampling

Patient enrollment in the current study was conducted as part of the NIH-funded *"Inflammation and the Host Response to Injury"* glue grant program. For trauma patients, inclusion criteria for the study population included: (1) blunt trauma patients with ages between 16 and 55; (2) an abbreviated injury scale (AIS) severity score greater than 2 outside the head region; (3) emergency department arrival less than 6 hours from the time of injury; (4) base deficit greater than 6 or systolic blood pressure less than 90 mmHg in prehospital care, or within 60 minutes of arrival; (5) blood transfusion within 12 hours of injury; and (6) intact cervical spinal cord. Patients were excluded if they had a prehospital Glasgow Coma Scale score of less than 8 or died within the first 48 hours of hospitalization. Burn patients met the following inclusion criteria: 0–89 years of age, admitted to a participating hospital within 96 hours after injury, and had burns covering more than 20% of total body surface area (TBSA) requiring at least one surgical intervention.

The microarray data presented in **Figure 4** of the main text was performed on neutrophil extracts from a cohort of trauma patients for which there were seven processed microarrays from neutrophils isolated over the 28 day sampling period, Demographic information for these patients is given in **Supplementary Table 12**.

For burn patients from the Massachusetts General Hospital (MGH) Burns Unit, inclusion criteria was: Age 18-80, burn size 20-90% total body surface area (TBSA), and pre-existing venous or arterial catheter.

Microfluidic device design and fabrication

Microfluidic devices in this study were designed to capture PMNs directly from whole blood under carefully controlled shear conditions [1,2]. Previous studies in our lab have shown that there is an optimal shear stress at which cells will adhere to an immunoaffinity capture surface [1]. We first measured this optimal shear stress by capturing PMNs in a Hele-Shaw parallel plate device, in which the fluid shear stress at the capture surface varies linearly along the length of the device [3]. The position in the Hele-Shaw chamber with the highest density of capture was used to determine the optimal shear stress for capture in subsequent studies. For a parallel plate capture chamber, the flow rate at a given shear stress and channel geometry can be approximated from the formula, $Q = \frac{\tau w h^2}{6\mu}$, where τ is the shear stress at the surface, μ is the dynamic viscosity, Q is the volumetric flow rate, and w and h are the width and height, respectively.

Rapid-prototyping methods were used to manufacture the polydimethyl siloxane devices[4,5]. Briefly, SU-8 photolithography was used to generate microstructured device features on silicon masters [6]. PDMS was poured over these featured and allowed to cure overnight at 65°C. These PDMS devices were then cut and de-molded from the masters, had inlet and outlet holes punched, and were irreversibly sealed to glass slides

following oxygen plasma treatment[5]. The channel surfaces were coated with a layer of covalently-attached Neutravidin (Pierce) [1], and a biotinylated capture antibody (AbD Serotec CD66b, clone 80H3) was added to the devices (20 μg/ml) to capture neutrophils. All general lab reagents used were Nuclease-free and sterile filtered. For the clinical studies, all reagents were lot tracked and stored separately from general lab supplies, and 1-5 devices from each production run were tested for cell capture. Devices were stored in a coldroom with no degradation in performance over a 12 month period, however, a two month expiration was employed for devices within the clinical sampling program.

Blood was pumped through the device using a syringe pump (Harvard Apparatus Pico series) held upright to minimize the effects of cell sedimentation in whole blood. For the Hele-Shaw device, blood was pumped at different flow rates corresponding to 0.2-5 dynes/cm^2. For immunofluorescent staining, cells were fixed with 4% paraformaldehyde (BD Bioscience Cytofix), blocked with 1% BSA in PBS, and stained with antibodies (1 μg/ml each BD Biosciences CD66-PE, CD14-APC, and CALTAG CD3-Alexa Flour 488) for 30 minutes. Following staining, nuclei were counterstained with DAPI (40 nM) for 15 minutes, and then flushed and stored in PBS until imaging. Wright-Giemsa (Sigma WS16, GS500) staining was also performed for bright field analysis of cells. Because both Wright and Giemsa stains can contain precipitates which clog the microfluidic channels, all solutions were passed through a 0.45 μm syringe filter prior to injection into the device. Non-specific esterase (Sigma) and Sudan Black (Sigma) staining was also performed to verify cell purity (data not shown).

RNA Extraction

Genomic processing of cells is accomplished by lysing the captured cells *in situ*. Briefly, following removal of unbound cells with nuclease-free PBS the device outlet tubing was replaced with a short length of clean Teflon tubing. For genomics, we adapted a standard RNA processing protocol from Qiagen; 350 μl standard guanadinium isothiocyanate (RLT buffer, Qiagen) was pushed though the device by hand using a 1 ml syringe. The lysate was collected into a Qiashredder column (Qiagen) and processed according to manufacturer recommendations. This lysate was then stored at -80°C awaiting RNA extraction. RNA was extracted using a Qiagen Mini Plus kit, according to kit protocols with the exception that 350 μl of RLT Plus buffer and 2-mercaptoethaol (Sigma) at 20 μl/ml was added to the lysate prepared above before adding to the gDNA column to extract genomic DNA from the cell lysate. This yielded purified total RNA, which was subsequently analyzed on an Agilent Bioanalyzer 2100 system. Absence of genomic DNA was verified with RT-PCR with and without the Reverse Transcriptase.

Proteomic processing of microfluidic-enriched neutrophils

For proteomics, following washing of the capture cassette and outlet tube replacement, the cells were lysed in a 50% v/v solution of trifluoroethanol (Fluka) in 25 mM ammonium bicarbonate buffer (pH 8.0) in a compact ultrasonic bath (Branson). Cell lysate was immediately frozen at -80 °C and shipped on dry ice for analysis.
The protein content in enriched PMN lysate samples in 50% (v/v) of 2,2,2-trifluoroethanol (TFE) were determined by a BCA protein assay (Pierce Biotechnology,

Inc., Rockford, IL). 2 mM dithiothreitol was added to the samples followed by incubation at 60 °C for 2 hours with gentle shaking at 300 rpm. The samples were then diluted 5-fold with 50 mM NH_4HCO_3, pH 7.8 and digested by sequence-grade porcine trypsin (Promega, Madison, WI) at a 1:50 enzyme: protein ratio (w/w) for three hours at 37 °C. The digested samples were then dried to 40 µL in a vacuum concentrator. Particulate was removed through ultracentrifugation at 80k rpm for 20 minutes at 4 °C.

Reversed-phase capillary LC-MS and MS/MS analyses

An aliquot of 1.25 µg peptides from each sample was injected for LC-MS analysis using a custom-built capillary LC system coupled online to a hybrid linear ion trap mass spectrometer (LTQ-Orbitrap; ThermoElectron) using an in-house manufactured electrospray ionization interface. The MS scan performed by the Orbitrap had a resolution of 60k with the top six ions chosen for MS/MS analysis by the LTQ (*m/z* 400-2,000) using a dynamic exclusion window of 1 min and a normalized collision energy of 35%.

Custom Affymetrix Human Exon-Junction (GG-H) Array

To study the human transcriptome response to injury, we custom-designed a 6.9 million feature Affymetrix human exon-junction array with on average 100+ unique probes targeting each of the annotated human genes. Briefly, using genome assembly of hNCBI36 and contents from RefSeq, Ensembl, UCSC Known Genes and Exonwalk (02/2008), we examined the ‘annotated’ genes and ‘observed’ transcripts in terms of exons and exon-exon junctions. This yielded a comprehensive collection of 335,663 unique transcripts, consisting of a total of 370,298 unique exons, and 260,488 exon-

exon junctions. The set of unique transcripts formed 34,834 transcript clusters (genes). On average 10 probes were designed per unique exon and 4-6 probes per exon-exon junction, resulting in more than 100 probes on average targeting each of the 34,834 genes (34,834 probe sets).

Genomic Data Analysis

For Affymetrix HU133 Plus 2.0 Array, a total of 54,675 probe sets were analyzed. Low level analysis was performed using dChip, and expression level was modeled using the perfect match only option [7]. Unique genes were identified from the probe sets with mapped Entrez GeneIDs (http://www.ncbi.nih.gov/Entrez/). For GG-H array, a total of 34,834 probe sets were analyzed using a custom Affymetrix Power Tools (APT) Software Package. Significance analysis of microarrays[8] was applied, on the basis of 1,000 permutations, to identify probesets significantly perturbed by LPS and GM+I (with false discovery rate of <0.01) and genes significantly changed by trauma injury over the 28 day time course (with false discovery rate of <0.001) as described previously[9]. For HU133 array, unique genes were identified from the probe sets with mapped Entrez GeneIDs (http://www.ncbi.nih.gov/Entrez/). The Ingenuity Pathways Analysis, was used to construct pathways and functional module as previously described [9].

LC-MS Dataset Analysis

The LC-MS datasets were automatically analyzed using an in-house developed software package that includes tools such as ICR2LS and VIPER[10]. Peptide identification was performed by matching the accurately measured masses and normalized elution time (NET) values of each detected feature to a pre-established AMT

tag database for human PMN. The PMN AMT tag database was generated from the two-dimensional LC-MS/MS shotgun profiling of pooled PMN samples from both healthy controls and trauma subjects. The peptide sequences of a given feature were assigned when the measured mass and NET for each given feature matched the calculated mass and NET of a peptide in the AMT tag database within a 2 ppm mass error and 2% NET error. The final processed data contain the peptide MS intensity values for each identified feature. The raw peptide intensity data was then converted into $\log_2$ format and the datasets were normalized by a central tendency approach. The peptide abundance profiles across the different conditions were then re-scaled and rolled up to protein level abundance by taking the mean abundances for those peptides mapping to each protein. Significant proteins between two biological conditions were identified by performing ANOVA test. P-values from ANOVA test comparing proteins under different conditions were then adjusted for false discovery rate <0.05 using Q-value [11].

References

1. X. Cheng, D. Irimia, M. Dixon et al., *J Acquir Immune Defic Syndr* **45** (3), 257 (2007).
2. S. K. Murthy, A. Sin, R. G. Tompkins et al., *Langmuir* **20** (26), 11649 (2004).
3. S. Usami, H. H. Chen, Y. Zhao et al., *Ann Biomed Eng* **21** (1), 77 (1993).
4. J. C. McDonald, D. C. Duffy, J. R. Anderson et al., *Electrophoresis* **21** (1), 27 (2000).
5. K. Kotz, X. Cheng, and M. Toner, *J Vis Exp* (8), 319 (2007).
6. P. Sethu, M. Anahtar, L. L. Moldawer et al., *Anal Chem* **76** (21), 6247 (2004).
7. C. Li and W. H. Wong, *Proc Natl Acad Sci U S A* **98** (1), 31 (2001).

8. V. G. Tusher, R. Tibshirani, and G. Chu, *Proc Natl Acad Sci U S A* **98** (9), 5116 (2001).

9. S. E. Calvano, W. Xiao, D. R. Richards et al., *Nature* **437** (7061), 1032 (2005).

10. J. S. Zimmer, M. E. Monroe, W. J. Qian et al., *Mass Spectrom Rev* **25** (3), 450 (2006).

11. John D. Storey, *Journal Of The Royal Statistical Society Series B* **64** (3), 479 (2002).